machines

MDPI

Article

Complete Coverage Path Planning for Wind Turbine Blade Wall-Climbing Robots Based on Bio-Inspired Neural Networks and Energy Consumption Model

Da Chen, Gang Yu * and Shuchen Huang

School of Mechanical Engineering and Automation, Harbin Institute of Technology (Shenzhen), Shenzhen 518000, China; 22s153197@stu.hit.edu.cn (D.C.); 22s053026@stu.hit.edu.cn (S.H.)
* Correspondence: gangyu@hit.edu.cn

Abstract: The rapid growth in the use of wind energy has led to significant challenges in the inspection and maintenance of wind turbine blades, especially as turbine sizes increase dramatically and as operational environments become harsh and unpredictable. Wind turbine blades, being the most expensive and failure-prone components, directly affect operational stability and energy efficiency. The efficient and precise inspection of these blades is therefore essential to ensuring the sustainability and reliability of wind energy production. To overcome the limitations of the existing inspection methods, which suffer from low detection precision and inefficiency, this paper proposes a novel complete coverage path planning (CCPP) algorithm for wall-climbing robots operating on wind turbine blades. The proposed algorithm specifically targets highly complex regions with significant curvature variations, utilizing 3D point cloud data to extract height information for the construction of a 2.5D grid map. By developing a tailored energy consumption model based on diverse robot motion modes, the algorithm is integrated with a bio-inspired neural network (BINN) to ensure optimal energy efficiency. Through extensive simulations, we demonstrate that our approach outperforms the traditional BINN algorithms, achieving significantly superior efficiency and reduced energy consumption. Finally, experiments conducted on both a robot prototype and a wind turbine blade platform validate the algorithm's practicality and effectiveness, showcasing its potential for real-world applications in large-scale wind turbine inspection.

Keywords: complete coverage path planning; wall-climbing robot; wind turbine blade; bio-inspired neural network; energy consumption model; 2.5D grid map

check for updates

Academic Editor: Davide Astolfi

Received: 26 January 2025
Revised: 19 February 2025
Accepted: 21 February 2025
Published: 24 February 2025

Citation: Chen, D.; Yu, G.; Huang, S. Complete Coverage Path Planning for Wind Turbine Blade Wall-Climbing Robots Based on Bio-Inspired Neural Networks and Energy Consumption Model. *Machines* **2025**, *13*, 180. https://doi.org/10.3390/machines13030180

Copyright: © 2025 by the authors. Licensee MDPI, Basel, Switzerland. This article is an open access article distributed under the terms and conditions of the Creative Commons Attribution (CC BY) license (https://creativecommons.org/licenses/by/4.0/).

1. Introduction

With the rapid expansion in the use of wind energy [1], the inspection and maintenance of wind turbines have become increasingly critical, particularly as turbine sizes grow [2] and as they operate in harsh environments such as offshore wind farms and deserts [3,4]. Among the turbine components, blades are the most challenging to inspect due to their large size, complex geometry, and exposure to environmental factors. These blades are not only the most expensive components—accounting for over 20% of the total turbine cost—but also the most vulnerable to damage. Defects such as scratches, coating damage, and cracks often occur during transportation, installation, or operation and can significantly impact energy efficiency, operational stability, and maintenance costs [5]. If undetected, such damage can escalate, resulting in severe accidents and higher repair costs [6]. Therefore,

early detection and timely maintenance of blade surface defects are essential to ensuring turbine reliability and safety.

Various inspection methods have been developed to address these challenges, including manual inspection, unmanned aerial vehicles (UAVs) [7], tower-climbing robots [8–10], and wall-climbing robots [11,12]. However, these methods face significant limitations. Manual inspections are labor-intensive and prone to human error, particularly when identifying small surface defects. UAV-based inspections, while capable of providing a broader view of the turbine, are constrained by camera resolution and often fail to detect subtle defects. Additionally, UAVs are unable to perform internal inspections of the blade structure, limiting their effectiveness [13]. Tower-climbing robots rely on blade rotation for full inspection, resulting in low efficiency and inconsistent detection quality. Wall-climbing robots, which can operate directly on the blade surface, offer a promising alternative for automated inspection; however, despite the advancements in their structural design and adhesion mechanisms, research on their localization and path planning capabilities remains limited. This restricts their ability to achieve high-efficiency, complete coverage inspections of the blade surface.

Path planning is a critical area for improving the performance of wall-climbing robots. Complete coverage path planning algorithms are widely applied in tasks such as cleaning [14,15], agricultural activities [16,17], and underwater exploration [18,19]. These algorithms aim to ensure full task coverage while improving operational efficiency. Existing complete coverage path planning algorithms are typically designed for flat or nearly flat surfaces, such as floors or walls. These algorithms are generally categorized into cell decomposition methods [20–23], template-based methods [24], and grid-based methods [25]. Cell decomposition methods lack flexibility when dealing with complex curved surfaces, while template-based methods rely heavily on prior environmental knowledge, making them unsuitable for dynamically changing blade surfaces. Grid-based methods typically utilize discretization for two-dimensional planes and are simple and straightforward, making them convenient for integration with sensor data. Therefore, this study adopts the grid-based method for the environmental modeling of wind turbine blades and utilizes it as the basis for complete coverage path planning. However, for three-dimensional curved surfaces like wind turbine blades, grid-based methods often fail to consider the significant variations in blade curvature and surface geometry, which can lead to increased path redundancy and higher energy consumption for the robot. Furthermore, the large size and complex structure of wind turbine blades impose additional challenges in optimizing robot motion to minimize energy usage while ensuring complete surface inspection. These challenges highlight the need for more advanced and efficient path planning algorithms tailored to the unique demands of wind turbine blade inspection.

Bio-inspired robot path planning methods have provided novel insights for addressing complex curved surface coverage challenges. Inspired by the locomotion strategies of biological organisms, researchers have developed frameworks based on ant colony optimization (ACO) [26] and genetic algorithms (GAs) [27]. For example, Chen et al. (2022) proposed a movement optimization framework for cyborg cockroaches [28], which employed machine learning to analyze the relationship between tactile feedback and terrain curvature in real time, significantly improving path coverage and energy efficiency in bounded spaces. Similarly, bionic snake robots have leveraged central pattern generator (CPG) models to achieve adaptive winding motions on 3D surfaces [29], while swarm robotic systems have addressed collaborative coverage in dynamic environments by mimicking bee colony behaviors [30]. However, the existing bio-inspired approaches still face the following two major challenges when applied to large-scale continuous surfaces such as wind turbine blades: First, locally optimized biological behavior rules struggle to globally

coordinate long-distance coverage paths; Second, the coupling between biomimetic motion patterns and complex surface geometry remains underdeveloped, leading to insufficient accuracy in energy consumption prediction. These limitations have driven researchers to explore hybrid solutions that integrate bio-inspired algorithms with structured environmental models. For instance, combining the machine learning strategies from cockroach movement optimization [28] with grid-based surface representations may offer more efficient solutions for scenarios like wind turbine blade inspection.

To address these issues, this study proposes a novel complete coverage path planning (CCPP) algorithm specifically designed for wall-climbing robots operating on the complex curved surfaces of wind turbine blades. The algorithm integrates an energy consumption model with an improved BINN approach to achieve energy-efficient path planning. By utilizing 3D point cloud data, the method identifies regions of high curvature variation, extracts key height information, and then constructs a 2.5D grid map for precise planning. Comparative simulations demonstrate the algorithm's superior efficiency and reduced energy consumption compared to traditional BINN methods. Furthermore, real-world experiments on a robot prototype confirm the algorithm's practicality and feasibility, highlighting its potential for industrial applications.

In summary, this study makes significant contributions to the field of CCPP for wall-climbing robots by introducing a novel algorithm that achieves both energy efficiency and high performance on complex curved surfaces. The proposed method has been rigorously validated through simulations and real-world experiments, demonstrating its superiority over existing approaches. The remainder of this paper is structured as follows: Section 2 details the methodology, including the task description, evaluation metrics, and algorithm design. Section 3 presents the simulation results, while Section 4 discusses experimental validation. Finally, Section 5 concludes the paper and outlines the future research directions.

2. Complete Coverage Path Planning Methodology for Blade Wall-Climbing Robots

2.1. Task Description and Evaluation Metrics

Surface defect detection on wind turbine blades is a critical process to ensure the safe operation of wind power systems. In this context, wall-climbing robots are required to perform complete coverage path planning on the complex geometric surfaces of wind turbine blades, enabling the systematic inspection of surface defects.

To achieve the complete coverage inspection of wind turbine blades, the wall-climbing robot must start from any single side of a blade and systematically traverse the entire surface through precise path planning. Upon completing the inspection of one side, the robot returns to the blade root and transitions across the root area to the opposite side for inspection. After inspecting both sides of a single blade, the robot moves along the outer surface of the hub to the root of the next blade and begins the inspection task for that blade. This process is repeated until all three blades of the wind turbine have been fully inspected. By completing the inspection of an entire wind turbine in a single operation, the robot avoids the time loss and deployment complexity associated with stepwise inspections. This approach significantly enhances inspection efficiency and reduces operation and maintenance costs.

Considering the gradient curvature characteristics of blades from root to tip, the robot must ensure stable adhesion while optimizing its path strategy to achieve complete coverage of the blade surface. This requires the robot to accurately perceive and adapt to dynamic changes in surface curvature, precisely localize itself in complex geometries, and record the spatial distribution of potential defects. Such capabilities provide reliable data for subsequent damage assessment and maintenance decision-making.

To fulfill the above objectives, the path planning algorithm must achieve an optimal balance among multiple performance metrics. These metrics directly affect the reliability and efficiency of the inspection task, determining the practical applicability of wall-climbing robots in engineering scenarios. Based on this, a comprehensive evaluation system has been established as follows [31]:

1. Coverage Rate: The percentage of the blade surface traversed by the robot, ensuring no areas are missed.
2. Energy Efficiency: The energy consumed to complete the full coverage path. This metric requires consideration of the robot's energy consumption behavior in regions with varying curvatures and should be optimized to extend operational endurance.
3. Path Length: The total length of the planned path, which should be minimized to improve efficiency.
4. Redundancy Rate: The proportion of repeatedly inspected areas relative to the total inspection area. While redundancy may be acceptable in critical regions to ensure detection accuracy, unnecessary repetition elsewhere should be avoided.

High coverage rate ensures comprehensive inspection, while low energy consumption, low redundancy rate, and short path length collectively enhance the robot's endurance, economic efficiency, and overall inspection effectiveness. By establishing this comprehensive evaluation system, it becomes possible to systematically assess the performance of path planning algorithms, providing scientific guidance for practical engineering applications.

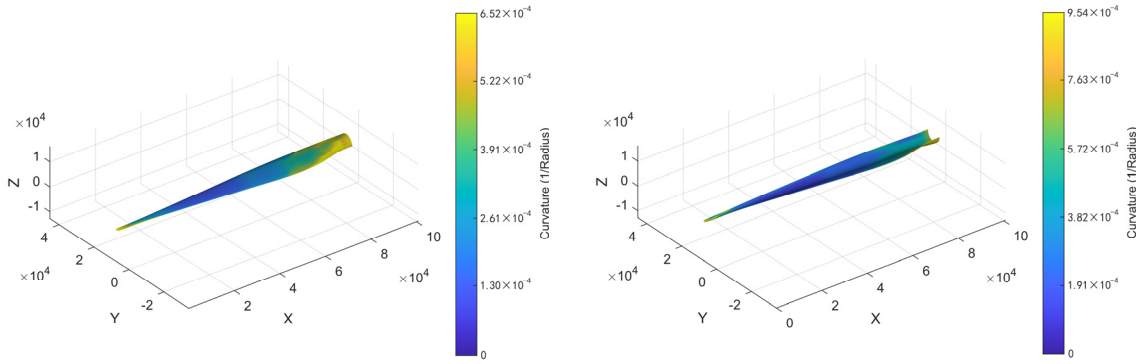
This study aims to optimize the complete coverage path planning algorithm for wall-climbing robots on wind turbine blades, improving their performance in surface defect detection. The findings of this research will provide robust support for the safe operation of wind power systems.

2.2. Analysis of Typical Operational Regions of Wind Turbine Blades

Wind turbine blades exhibit complex curvature variations, which have a direct impact on the adhesion capability and mobility efficiency of wall-climbing robots. In regions with higher curvature, robots may encounter difficulties in maintaining stable adhesion, as well as challenges in path planning. Complete coverage path planning must ensure that the robot efficiently traverses the entire blade surface without missing any areas. By analyzing the curvature variations, it is possible to identify critical regions, thereby optimizing path planning strategies to enhance the accuracy and efficiency of inspection and maintenance processes.

To simulate the working environment on actual wind turbine blades, it is essential to focus on regions with higher curvature, where wall-climbing robots face greater challenges in adhesion, based on the calculated results and structural design requirements. Considering the large size of wind turbine blades and their complex surface curvature variations, identifying and analyzing high-curvature regions is critical for addressing adhesion and path planning issues. The curvature at each point should be calculated to pinpoint these challenging areas. The curvature variations on the surface of wind turbine blades are illustrated in Figure 1. Brightly colored regions, which exhibit significant curvature changes, often represent bottlenecks in path planning.

As shown in Figure 1a, the curvature of the upper blade surface is relatively small, with regions of higher curvature primarily concentrated near the blade root and the blade tip. Figure 1b displays the curvature of the lower blade surface. Compared to the upper surface, the lower blade exhibits slightly higher curvature and should therefore be prioritized as a focus area for planning and optimization.



(**a**) (**b**)

Figure 1. The curvature variations on the surface of wind turbine blades. (**a**) The curvature of the upper blade surface. (**b**) The curvature of the lower blade surface.

Wind turbine blades exhibit two typical types of early-stage damage, as shown in Figure 2. The high-curvature blade tip region is prone to erosion damage, while the lower-curvature region, extending from the blade root to approximately two-thirds of its length, is more susceptible to cracking.

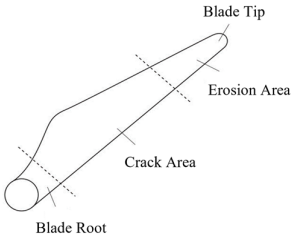
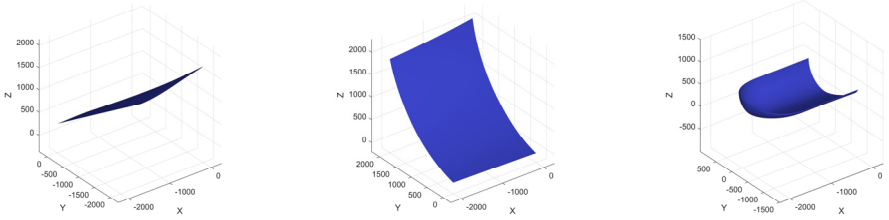


Figure 2. The vulnerable regions of the blade.

Based on the damage characteristics and curvature distribution, this study identifies the typical working regions of the wind turbine blade, as shown in Figure 3. Figure 3a illustrates the typical curved surface near the blade root, where significant curvature variation poses major challenges for the path planning of wall-climbing robots. Figure 3b depicts the typical curved surface in the middle section of the blade, where curvature variation is relatively small but cracking is more likely to occur, and this region occupies the largest surface area. Figure 3c shows the typical curved surface at the blade tip, where drastic curvature changes make this region highly prone to erosion.



(**a**) (**b**) (**c**)

Figure 3. The three typical regions of the blade extracted. (**a**) Blade root Region. (**b**) Blade middle region. (**c**) Blade tip region.

Through the analysis of the surface characteristics of wind turbine blades, it is evident that although the three typical regions of the blade surface differ in common early defect types and curvature complexity, issues such as drastic curvature changes and large inspection areas across the blade surface pose challenges to the full coverage path planning

of wall-climbing robots. To address these challenges, improvements in the full coverage path planning algorithm for wall-climbing robots are proposed, based on the structural characteristics of wind turbine blades. These improvements will effectively enhance the overall efficiency and reliability of blade inspection and maintenance tasks.

2.3. Construction of the 2.5D Grid Map for Blade Surface Modeling

In full coverage path planning tasks, traditional 2D grid maps typically only include planar positional information, which fails to adequately reflect the complexity of real environments. In practical applications, environments are often three-dimensional, featuring various height variations such as slopes, steps, and obstacles. These height variations have a significant impact on path planning, and neglecting height information may result in planned paths being infeasible in practice or even pose safety risks. Generally, robot full coverage path planning only considers positional changes in the 2D coordinates.

In this study, considering the specific nature of the working environment, the surface of wind turbine blades is not a flat plane but instead exhibits certain height and curvature variations. As a legged wall-climbing robot moves across the surface of a wind turbine blade, its motion must be integrated with its adhesion mechanism. By taking height information into account, paths can be planned more precisely to reduce redundant coverage and missed areas, thereby improving task efficiency and resource utilization.

A 2D grid map is a representation of a continuous space converted into a discrete structure. It divides the environment into equal-sized square grid cells, with each grid cell corresponding to a portion of the real-world environment. During path planning, the occupancy state of each cell is represented using binary values as follows: 0 indicates uncovered space, while 1 represents either an obstacle (infeasible space) or an already traversed (covered) space. Additionally, the map can store more detailed information, which can be indexed and accessed using a 2D array of row–column coordinates.

A 2.5D grid map, as defined and utilized in the previous section, extends the concept of 2D grid maps by incorporating height information into the grid cells. For path planning, it is necessary to supplement the grid with occupancy states based on this height data. By integrating height information, the curvature changes of the blade surface can be indirectly represented, allowing the robot's path planning algorithm to choose the optimal path. This avoids unnecessary ascents or descents, improves planning efficiency, and reduces energy consumption. Consequently, this approach enhances the robot's endurance and operational efficiency.

The correspondence between 2D grid maps and bio-inspired neural networks (BINNs) is illustrated in Figure 4. A 2D neural network is constructed based on the 2D grid map, where each grid cell in the map is represented by a neuron in the neural network. The connections between neurons indicate the ability of a neuron to perceive its neighboring neurons. Each neuron can sense other neurons within a neighborhood defined by a specific radius and determines the next movement direction based on the activation values of the neurons [32].

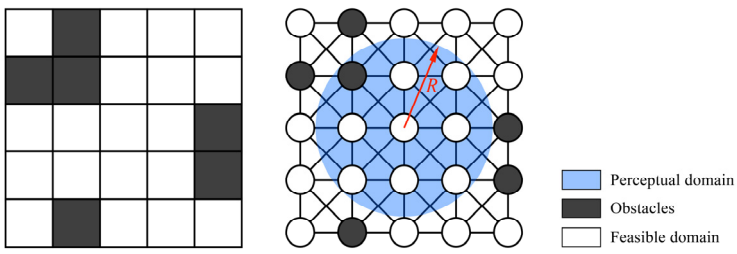
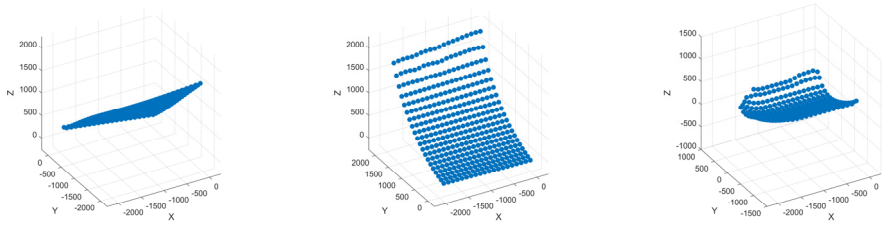


Figure 4. The Correspondence Between 2D Grid Maps and Bio-Inspired Neural Networks.

In wind farms, the 3D models of wind turbines are typically known; however, the curved surfaces of wind turbine blades are not regular surfaces that can be represented using equations. By discretizing the 3D models, point cloud data of the blade surfaces can be obtained. The height information at various positions on the blade can be extracted through point cloud data.

To construct a 2.5D grid map for the proposed typical regions, the process begins by discretizing the environmental map into grid cells. This involves dividing the continuous space into a uniform grid structure, where each cell represents a small, discrete portion of the environment. Each grid cell is then assigned a value that corresponds to its occupancy state, such as free space, occupied space, or unknown space. This step results in the creation of a foundational 2D grid map, which provides a simplified representation of the environment in terms of occupancy.

Building upon this 2D grid map, height information is incorporated for each grid cell to supplement the data and enhance the map's dimensionality. Specifically, the height of each grid cell is determined by sampling the surface of the environment within the boundaries of the cell. This height sampling process is carried out according to the grid resolution, with the smaller grid sizes capturing the finer details of the environment. For the three proposed types of typical regions, height sampling generates a point cloud map that represents the surface geometry of these regions, as illustrated in Figure 5.



(**a**) (**b**) (**c**)

Figure 5. Acquisition of Grid Height Information. (**a**) Point Cloud of the Root Typical Region. (**b**) Point Cloud of the Middle Typical Region. (**c**) Point Cloud of the Tip Typical Region.

The height value corresponding to each grid cell is then stored as an additional attribute in the grid map. This step effectively transforms the 2D grid map into a 2.5D grid map, where each cell not only contains occupancy information but also possesses height data that reflects the elevation of the environment at that specific location. By combining occupancy states and height information, the 2.5D grid map provides a richer and more comprehensive representation of the surface geometry of the environment.

As a result, the final 2.5D grid maps for the three typical regions are constructed, capturing both the horizontal and vertical characteristics of each region. These maps, as shown in Figure 6, serve as a valuable resource for detailed analysis, path planning, and other applications which require an understanding of both surface topology and spatial constraints.

In the task of complete coverage path planning, grid cells are classified into three states—uncovered, covered, and obstacle—with their priority levels decreasing in this order. Each grid cell can belong to only one state at a time. Traversal of every uncovered cell is ensured by detecting each grid cell.

Within the working area, the wind turbine blade itself does not contain inaccessible obstacle cells. However, during the motion of the wall-climbing robot, to avoid secondary damage to defects caused by the robot's adhesion, the blade can be treated as a locally unknown grid map. Grid cells identified as defects are treated as obstacle cells. The robot

continuously collects local environmental information and updates it to the global map, thereby achieving the complete coverage task across the blade area.

358	345	331	318	304	291	277	264	250	236	222	208	194	180	166	151	137	123	109	94
395	382	369	355	342	329	315	302	288	274	261	247	233	218	204	190	175	161	147	132
468	456	443	430	418	405	391	378	365	351	338	324	310	296	282	268	254	239	225	210
542	530	518	506	493	481	468	455	442	429	416	403	389	375	361	348	334	320	305	291
616	605	593	581	570	558	545	533	521	508	495	482	469	456	443	429	415	402	388	373
691	680	669	657	646	635	623	612	600	588	576	563	551	538	525	512	498	485	472	458
764	754	744	733	723	712	701	690	679	668	656	645	633	621	608	596	583	571	558	545
837	828	819	809	799	790	779	769	758	748	737	726	716	705	693	681	669	657	645	633
910	901	893	884	875	867	857	848	837	828	819	808	799	789	778	767	756	745	734	723
981	973	966	958	951	943	934	926	917	909	900	891	882	872	863	854	843	834	824	813
1051	1045	1039	1032	1025	1018	1011	1004	996	989	981	973	965	957	949	940	931	923	914	905
1121	1115	1110	1104	1099	1093	1087	1081	1075	1068	1062	1055	1048	1041	1034	1027	1019	1012	1004	997
1189	1184	1180	1176	1171	1166	1161	1156	1152	1146	1141	1136	1131	1125	1119	1113	1107	1101	1095	1089
1255	1252	1249	1245	1242	1238	1235	1231	1227	1224	1220	1216	1212	1208	1204	1199	1195	1190	1186	1181
1320	1318	1316	1314	1311	1309	1307	1304	1302	1300	1297	1295	1292	1290	1287	1284	1282	1279	1275	1273
1384	1382	1381	1381	1379	1378	1378	1376	1376	1374	1374	1373	1372	1371	1370	1368	1368	1366	1365	1364
1446	1446	1446	1446	1446	1446	1447	1447	1447	1448	1448	1449	1449	1450	1451	1452	1453	1453	1453	1454
1506	1507	1508	1510	1511	1512	1514	1516	1518	1520	1522	1524	1526	1528	1531	1534	1536	1539	1541	1544
1565	1567	1569	1572	1574	1577	1580	1583	1586	1590	1594	1598	1601	1606	1610	1614	1619	1624	1629	1634
1621	1625	1628	1632	1636	1640	1645	1649	1654	1659	1665	1671	1677	1683	1689	1696	1704	1711	1719	1728

(**a**)

1758	1775	1785	1784	1779	1792	1811	1818	1820	1818	1828	1850	1863	1871	1881	1894	1905	1914	1916	1912
1529	1550	1559	1555	1541	1552	1575	1576	1572	1561	1569	1592	1602	1606	1613	1623	1629	1632	1627	1612
1334	1342	1345	1347	1343	1346	1355	1355	1355	1352	1355	1363	1367	1370	1374	1378	1382	1384	1385	1384
1168	1169	1171	1172	1173	1174	1176	1177	1178	1180	1181	1183	1185	1187	1189	1191	1193	1195	1198	1200
1031	1031	1032	1032	1033	1033	1034	1035	1035	1036	1037	1038	1039	1040	1041	1042	1044	1045	1047	1049
909	909	909	909	909	909	909	909	910	910	910	911	911	912	912	913	914	915	916	917
801	800	800	799	799	798	798	798	798	798	797	798	798	798	798	798	798	799	799	800
703	702	701	701	700	699	699	698	698	697	697	696	696	696	695	695	695	695	695	695
615	613	612	611	610	610	609	608	607	606	606	606	605	604	604	603	603	602	602	601	601
534	533	532	531	530	528	527	526	525	524	523	522	522	521	520	519	518	518	517	516
462	460	459	458	457	455	454	453	451	450	449	448	447	446	445	444	443	442	441	440
396	394	393	391	390	389	387	386	384	383	382	380	379	378	377	375	374	373	372	371
336	334	333	331	330	328	326	325	323	322	320	319	317	316	315	313	312	310	309	308
281	280	278	276	275	273	271	270	268	267	265	263	262	260	259	257	255	254	253	251
232	231	229	227	225	224	222	220	219	217	215	213	212	210	208	207	205	203	202	200
188	187	185	183	181	180	178	176	174	172	171	169	167	165	163	161	160	158	156	154
149	147	145	144	142	140	138	136	134	133	131	129	127	125	123	121	119	117	115	113
114	112	110	109	107	106	104	102	100	98	96	94	92	90	88	86	84	82	80	77
83	81	80	78	76	75	74	73	71	68	65	63	61	59	57	55	54	52	49	46
57	55	53	52	50	48	47	46	44	41	38	36	34	32	30	28	26	24	22	19

(**b**)

					352	321	311	309	309	308	307	306	308	342	377	383	388	393	341
			270	267	268	245	237	236	236	235	234	233	233	250	267	272	273	272	244
		254	215	168	142	129	124	123	123	123	122	121	120	118	117	119	117	111	109
	259	190	130	96	76	65	61	61	60	60	60	59	58	57	55	54	52	50	48
281	222	134	86	57	40	31	28	27	27	27	26	25	24	23	22	21	19	17	15
229	183	111	69	43	27	19	16	16	15	15	15	14	13	12	11	9	8	6	4
220	179	113	74	50	35	28	25	24	24	23	23	22	21	20	19	18	16	14	12
238	198	135	96	72	58	50	47	47	46	46	45	44	44	42	41	40	38	36	34
272	231	166	128	103	89	81	78	78	77	77	76	75	74	73	72	70	69	67	65
314	271	204	165	140	125	117	114	114	113	113	112	111	111	109	108	107	105	103	101
362	318	248	207	181	166	158	155	154	154	154	153	152	151	150	149	148	146	144	142
422	373	297	254	227	211	203	200	199	199	199	198	197	197	195	194	193	191	190	188
	406	352	306	278	261	253	250	249	249	248	248	247	246	245	244	243	241	240	238
		394	366	335	317	308	304	304	304	303	303	302	301	300	299	298	297	295	294
			418	403	381	371	367	366	366	366	365	365	364	363	362	361	360	359	357
				441	416	405	401	400	400	400	399	399	398	397	396	395	394	393	432

(**c**)

Figure 6. 2.5D Grid Maps. (**a**) 2.5D Grid Map of the Root Typical Region. (**b**) 2.5D Grid Map of the Middle Typical Region. (**c**) 2.5D Grid Map of the Tip Typical Region.

2.4. Establishment of the Energy Consumption Model for Wall-Climbing Robots

When performing operations on wind turbine blades, the massive size of the blades and the limited mobility of the wall-climbing robot necessitate the effective management of

the robot's operational endurance. The robot's energy consumption directly impacts its working efficiency and continuous operational time. To ensure safe and efficient operation, it is critical to manage and optimize the robot's energy usage during the complete coverage defect detection task on the turbine blade.

Firstly, establishing an energy consumption model allows for a precise prediction of the energy required for the robot to complete the full coverage defect detection task on the turbine blade. This ensures that the robot operates within a safe energy consumption range, preventing potential safety hazards such as adhesion failure or falling due to excessive energy consumption. Secondly, the energy consumption model provides valuable guidance for path planning. By analyzing the energy consumption of different paths, the model enables the selection of the most energy-efficient path, ensuring that the robot can effectively complete blade inspection and maintenance tasks while conserving energy.

To achieve rational full coverage path planning for the wall-climbing robot, it is necessary to establish a comprehensive energy consumption model. The wall-climbing robot designed in this study uses a four-legged air pump adsorption mechanism for adhering to the surface of the wind turbine blade. The motion schematic of the single-leg mechanism is shown in Figure 7, where each rotational joint is driven by a ZP35D servo motor, sourced from Zhongling Technology, located in Hangzhou, China.

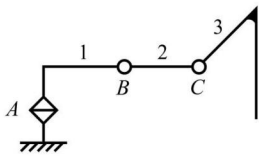


Figure 7. The motion schematic of the robot's single-leg mechanism.

The robot's energy consumption during the inspection of the turbine blade surface primarily arises from the following two components:

- Control System Energy Consumption: This includes the power required to manage sensors, onboard computing systems, and communication modules.
- Motion System Energy Consumption: This encompasses the energy consumed by robotic actuators, including the servo motors and the air pump system used for surface adhesion.

Considering these two major sources of energy consumption, the model can accurately estimate the robot's energy usage during various operations. This provides a foundation for optimizing the robot's path planning and ensuring its ability to complete the detection task effectively while avoiding the risks related to energy depletion.

As shown in Figure 8, the wall-climbing robot is capable of moving in eight directions. Its primary motion modes can be categorized into the following:

- Rotation Mode;
- Linear Movement Mode.

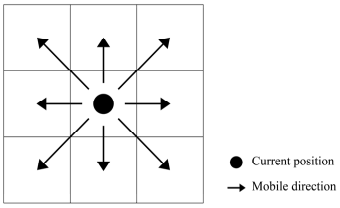


Figure 8. Robot Movement Directions.

The robot's movement in any of the eight directions can be decomposed into a combination of these two motion modes. Let the time required for the robot to perform a rotation be denoted as t_r, and the time required for the robot to perform linear movement in a straight direction be denoted as t_s.

The robot's energy consumption can be further detailed as follows:

- The power of the robot's control module is represented by P_c.
- The energy consumed by the control module is represented as E_c.
- The energy consumed by the robot's motion module is represented as E_m.
- The robot's total energy consumption is denoted as E_{sum}

$$E_{sum} = E_c + E_m = P_c(t_r + t_s) + E_m \tag{1}$$

Since the movement of the wall-climbing robot in any of the eight directions can be decomposed into a combination of rotation mode and linear movement mode, the energy consumption for rotation mode is denoted as E_r, while the energy consumption for linear movement mode is denoted as E_s, in the following equation:

$$E_m = E_r + E_s \tag{2}$$

The magnitudes of E_r and E_s are primarily influenced by the rotation angle α, the linear movement distance d, and the height difference between two adjacent grids Δh, as expressed by the following:

$$E_m = E_r(\alpha, d, \Delta h) + E_s(\alpha, d, \Delta h) \tag{3}$$

Let the rotation angles of joints A, B, and C be denoted as θ_1, θ_2, and θ_3, respectively. To ensure the end-effector remains in a vertical orientation at all times, it is required that the rotation angles of joint C and joint B are equal in magnitude but opposite in direction, i.e., $\theta_3 = -\theta_2$. The lengths of links 1, 2, and 3 are denoted as l_1, l_2, and l_3, respectively. The geometric relationship of the single-leg mechanism is illustrated in Figure 9.

$$\alpha = \theta_1 \tag{4}$$

$$d = l_1 sin\theta_1 \tag{5}$$

$$\Delta h = l_2 sin\theta_2 \tag{6}$$

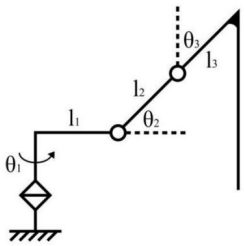


Figure 9. Geometric Relationship of the Robot's Single-Leg Mechanism.

When the wall-climbing robot operates in the rotation mode, the rotation angle α corresponds to the rotation angle θ_1 of joint A, and the linear movement distance $d = 0$. The angles θ_{r2} and θ_{r3} are set as fixed values. When $\theta_{r1} \neq 0$, the wall-climbing robot executes the rotation mode effectively; otherwise, all angles are set to zero. A very small positive number ϵ is used for control purposes. The rotation angles of the joints can then be expressed as follows:

$$\theta_{r1} = \alpha \tag{7}$$

$$\theta_{r2} = (\pi/6) \times (|\theta_{r1}|/|\theta_{r1}| + \in) \tag{8}$$

$$\theta_{r3} = -(\pi/6) \times (|\theta_{r1}|/|\theta_{r1}| + \in) \tag{9}$$

When the wall-climbing robot operates in the linear movement mode, the rotation angle α is determined based on the required linear movement distance d. The rotation angle θ_{s2} of joint B is determined by the height difference between two adjacent grids. The rotation angles of the joints can then be expressed as follows:

$$\theta_{s1} = sin^{-1}(d/l_1) \tag{10}$$

$$\theta_{s2} = sin^{-1}(\Delta h/l_2) \tag{11}$$

$$\theta_{s2} = -sin^{-1}(\Delta h/l_2) \tag{12}$$

Thus, the energy consumption of the motion module for the wall-climbing robot can be expressed as follows:

$$E_m = E_r + E_s = \sum_{i=1}^{3} E_{ri} + \sum_{i=1}^{3} E_{si} = \sum_{i=1}^{3} \left(\frac{\tau \times \theta_{ri}}{\tau} \right) + \sum_{i=1}^{3} \left(\frac{\tau \times \theta_{si}}{\tau} \right) \tag{13}$$

The torque of the servo motor used is $\tau = 3.5$ N·m, and the efficiency of the servo motor is $\eta = 0.7$. The rotation time of the servo motor is fixed at 2 s. The robot has four legs, and during the movement of a single grid, the legs on two diagonal lines alternately operate. Each leg performs two actions—lifting and lowering. Based on this, the total energy consumed by the wall-climbing robot to move in any of the eight possible directions can be expressed as follows:

$$E_{\text{sum}} = P_c(t_r + t_s) + E_m = 8P_c + 4(\tau/\eta) \sum_{i=1}^{3} (\theta_{ri} + \theta_{si}) \tag{14}$$

By constructing the energy consumption model of the robot, it becomes possible to quantify the energy required to move to the grid corresponding to the surrounding neurons. This model incorporates factors such as the distance difference, angle difference, and height difference required for movement. These parameters are then utilized to select the next grid for movement, enabling further optimization of the robot's path planning.

2.5. Design of the CCPP Algorithm Based on the Energy Consumption Model and BINN

The robot's path planning algorithm can be categorized into the following two types: point-to-point path planning and area coverage path planning. Area coverage path planning aims to design a path that allows the robot to efficiently and comprehensively cover a designated area to accomplish its task.

For surface defect detection on wind turbine blades, the climbing robot must traverse all the feasible regions on the blade. The algorithm should aim to minimize repetition, path length, and energy consumption as much as possible. This optimization improves the robot's endurance and enhances its detection efficiency, ensuring that the entire surface is inspected effectively.

A bio-inspired neural network (BINN) is employed for the complete coverage path planning. Its principle is inspired by the behaviors of biological systems, utilizing a neural network model to enable robots to perform autonomous navigation and coverage tasks in complex environments. BINN is frequently applied to collision-free path planning for robots in dynamic environments. Compared with other methods, BINN is a highly adaptive bio-inspired algorithm capable of effectively handling complex and dynamic environments without requiring a learning process.

BINN uses the activity and interactions of neurons to simulate the navigation mechanisms of biological organisms, thereby exhibiting adaptive and dynamic planning capabilities. The neuronal neighborhood network model of BINN is shown in Figure 10, where the following representations are used:

- Black neurons represent obstacles;
- White neurons represent feasible regions;
- The blue circular area, centered on the current neuron with a radius R, represents the perception domain. Neurons within this perception domain can influence the current neuron.

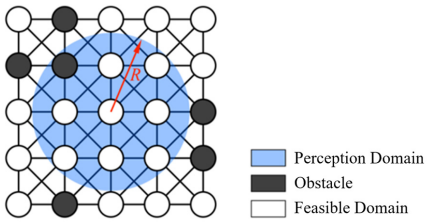


Figure 10. Neuronal Neighborhood Network Model.

The activity value of a neuron is determined by the shunting equation described in [33], as follows:

$$\frac{dX_i}{dt} = -AX_i + (B - X_i)\left[[I_i]^+ + \sum_{j=1}^{n} \omega_{ij}[X_j]^+\right] - (D + X_i)[I_i]^- \tag{15}$$

where X_i is the activity value of the i-th neuron, A is the decay rate of the neuron activity, B and D are the upper and lower limits of the neuron activity, respectively, n represents the number of neurons within the perception domain of radius R around the i-th neuron, ω_{ij} is the connection weight between the i-th neuron and the j-th neuron, and I_i is the external input, which can be calculated using Equation (16) [34].

$$I_i = \begin{cases} E, & \text{Uncovered area} \\ -E, & \text{Obstacle area} \\ 0, & \text{Covered area} \end{cases} \tag{16}$$

where E is a very large constant. The value of E is much greater than B, ensuring that the maximum activity value of uncovered neurons exceeds the minimum activity value of obstacle neurons. The term $[I_i]^+ + \sum_{j=1}^{n} \omega_{ij}[X_j]^+$ collectively represents a positive excitation to the neuron's activity, while $[I_i]^-$ represents a negative inhibition to the neuron's activity. Their functions are expressed as follows [35]:

$$[I_\mathrm{i}] = \begin{cases} \max\{I_\mathrm{i}, 0\}, [I_\mathrm{i}] = [I_\mathrm{i}]^+ \\ \max\{-I_\mathrm{i}, 0\}, [I_\mathrm{i}] = [I_\mathrm{i}]^- \end{cases} \tag{17}$$

The connection weight ω_{ij} is defined as follows [35]:

$$\omega_{ij} = \begin{cases} \frac{\mu}{d_{ij}}, & \text{The } j\text{-th neuron is within the perceptual domain} \\ 0, & \text{The } j\text{-th neuron is outside the perceptual domain} \end{cases} \tag{18}$$

where d_{ij} is the Euclidean distance between the i-th neuron and the j-th neuron, and μ is a constant.

Generally, the activity value of the current neuron is influenced by the activity values of all other neurons within its perception domain. Uncovered areas attract the robot to move,

while obstacle areas repel the robot to avoid collisions. Traditional BINN path planning algorithms are typically based on 2D grid maps, where a priority heuristic formula is used to comprehensively consider the impact of movement distance costs and robot turning angle costs. However, for the 3D environment in this paper, we consider the blade surface, height data, and the energy consumption model for various robot movement modes. On the basis of a 2.5D grid map, the algorithm comprehensively takes into account movement distance costs, turning angle costs, height difference costs, and energy consumption costs to determine the changes in neuron activity values [36]. Thus, the next movement target point for the robot is selected. The position of the robot's next target point P_n is obtained through X_n, which is expressed as follows [37]:

$$X_n = \max\{X_k + cY_k, k = 1, 2, \ldots, m\} \tag{19}$$

where c is a non-negative correction coefficient between 0 and 1, and Y_k is the influence variable obtained by considering various factors comprehensively.

c is used to proportionally adjust the influence value Y_k. If c is too small, the consideration of influencing factors for the target point becomes insignificant. If c is too large, the original neuron activity cannot dominate, and the robot may fail to achieve proper full coverage. Y_k is a variable obtained by comprehensively considering the movement distance, turning angle, height difference, and energy consumption difference between the current grid and the potential next grid. Y_k can be expressed as follows:

$$Y_{\mathrm{k}} = \frac{\alpha_1 y_d + \alpha_2 y_\theta + \alpha_3 y_h + \alpha_4 y_e}{4} \tag{20}$$

where α_1 is the influence coefficient of the distance between the robot's current grid and the potential next grid, α_2 is the influence coefficient of the turning angle between the robot's current grid and the potential next grid, α_3 is the influence coefficient of the height difference between the robot's current grid and the potential next grid, and α_4 is the influence coefficient of the energy consumption difference between the robot's current grid and the potential next grid. The magnitude of the influence coefficients determines the degree of importance the robot assigns to each factor when selecting the next target point, as follows:

$$y_d = 1 - \frac{\Delta d}{d} \tag{21}$$

where Δd is the Euclidean distance between the current grid and the potential next grid, and d is the maximum possible Euclidean distance between the current grid and the potential next grid.

$$y_\theta = 1 - \frac{\Delta \theta}{\pi} \tag{22}$$

where $\Delta\theta$ is the turning angle between the current grid and the potential next grid.

$$y_h = 1 - \frac{\Delta h}{h} \tag{23}$$

where Δh is the height difference between the current grid and the potential next grid, and h is the maximum possible height difference between the current grid and the potential next grid.

$$y_{\mathrm{e}} = 1 - \frac{\Delta E}{E} \tag{24}$$

where ΔE is the energy difference between the current grid and the potential next grid, and h is the maximum possible energy difference between the current grid and the potential next grid.

The improved BINN full coverage path planning process is shown in Figure 11. The input consists of map information and robot positioning information, while the output is the complete path. After initializing the input information, a 2.5D grid map of the wind turbine blade is created, and the BINN neural network is constructed to represent the occupancy status of grid cells. The robot starts area coverage from the initial position and updates the activity values of the neighboring neurons based on the priority heuristic formula to determine the next target grid cell. After the robot moves to the target grid cell, the cell becomes the current grid cell and is marked as covered, while the grid map is updated. When all eight grids surrounding the robot have been traversed, it indicates that the robot is in a deadlock. If the robot is in a deadlock and the grid map has been fully traversed, the detection ends; otherwise, point-to-point path planning is used to escape to a nearby unexplored grid cell to continue detection until all the grid cells are traversed.

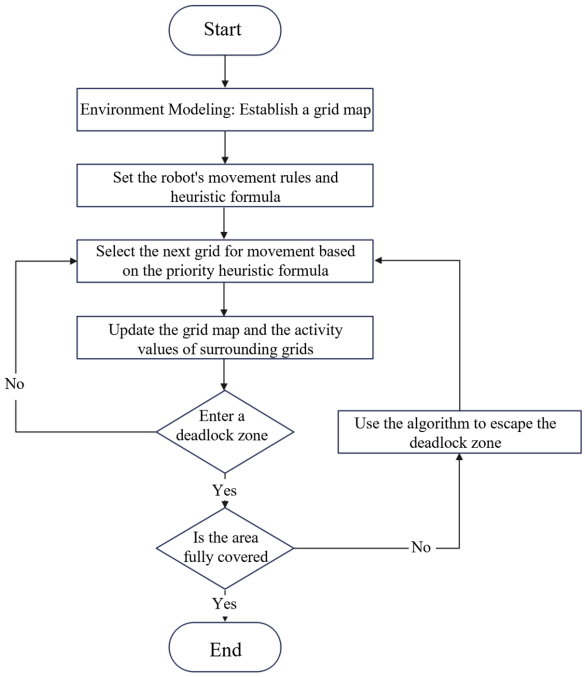


Figure 11. Flowchart of BINN Full Coverage Path Planning Based on Energy Consumption Model.

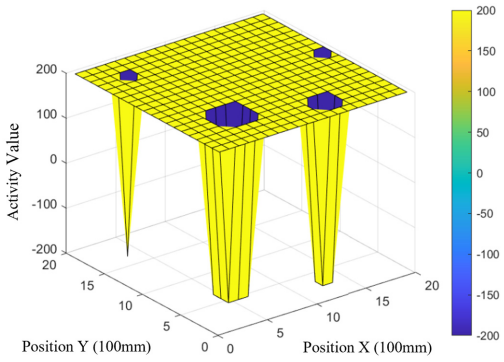
3. Simulation and Results

For the wall-climbing robot designed for wind turbine blade inspection, its working range covers both the upper and lower surfaces of the blade near the root. The curvature of the blade root changes uniformly. After completing the inspection of one side of the blade surface, the robot returns to the root of the blade to cross over and move to the other side for inspection. Therefore, simulation analysis of path planning is performed separately for the upper and lower surfaces of the wind turbine blade.

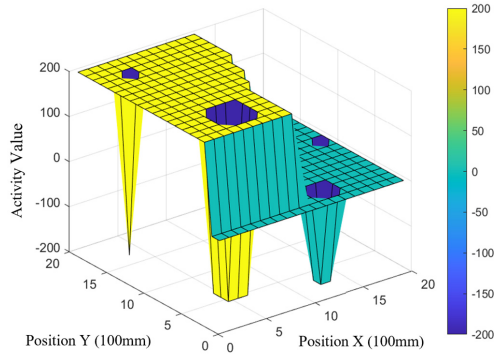
By proportionally scaling a typical middle section of the blade, a 2.5D grid map is constructed as the simulation environment for the robot. The total area is 2000 × 2000 mm, divided into a 20 × 20 grid, with each grid cell measuring 100 × 100 mm. In the grid map, the horizontal axis represents the physical quantity “Position X” (unit: 100 mm), indicating consecutive positions in the horizontal direction of the map, where each unit corresponds to a physical distance of 100 mm. Similarly, the vertical axis represents the physical quantity “Position Y” (unit: 100 mm), also indicating consecutive positions in the horizontal direction of the map, with each unit corresponding to a physical distance of 100 mm.

The robot starts moving from the same initial position and stops when all the grid cells have been traversed. The performance of the original BINN algorithm and the improved energy-consumption-based BINN algorithm was compared.

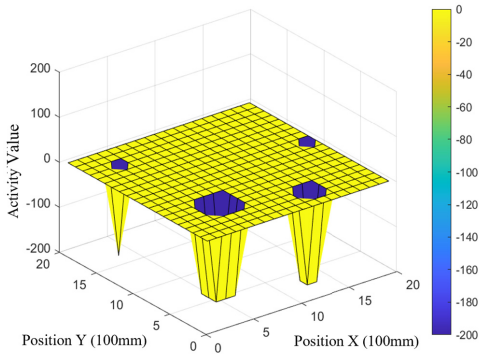
Simulations of the robot's traversal on the grid map were conducted using both the current BINN algorithm and the energy-consumption-based BINN algorithm. Both algorithms successfully completed the full coverage path planning. In the schematic diagram of neuron activity, the physical quantities and units of the horizontal and vertical axes are the same as those of the grid map, while the *Z*-axis represents the activity value of the neurons, which has no unit. The activity values of obstacles remain constant at −200, the initial activity value of uncovered areas is 200, and the activity value becomes 0 after being covered. The activity values before the area traversal begins are shown in Figure 12a. The changes in neuron activity during the traversal process are shown in Figure 12b, and Figure 12c shows the neuron activity after the grid traversal is completed.



(**a**)



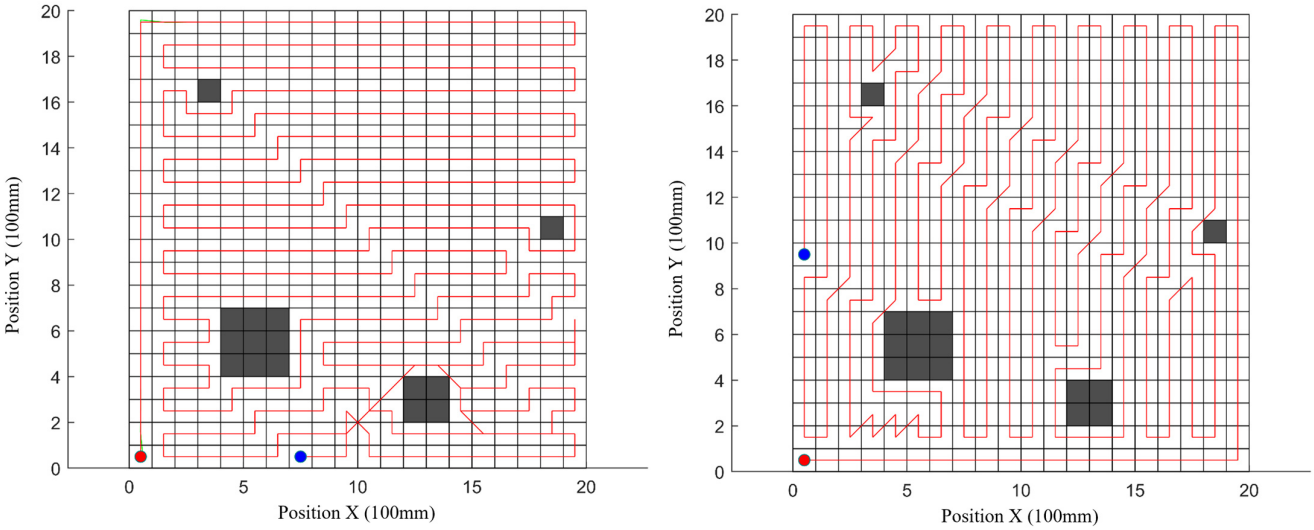
(**b**)



(**c**)

Figure 12. Variations in neuron activity. (**a**) Neuron activity before traversal. (**b**) Neuron activity during traversal. (**c**) Neuron activity after traversal.

Considering that the middle section of the blade accounts for the largest proportion of the blade's total surface area, it was selected as the simulation region. Simulations were conducted on a 2.5D grid map with height information using both the traditional BINN algorithm and the improved BINN algorithm. Through the simulations, the full coverage path of the traditional BINN algorithm was obtained, as shown in Figure 13a. The full coverage path of the energy-consumption-improved BINN algorithm was obtained, as shown in Figure 13b.



(**a**) (**b**)

Figure 13. Comparison of Movement Paths Between Two BINN Algorithms. (The red circle indicates the starting point, and the blue circle indicates the endpoint.) (**a**) Traditional BINN algorithm movement path. (**b**) Improved BINN algorithm movement path.

Simulation results provided evaluation data for the traditional BINN algorithm and the energy-consumption-based improved BINN algorithm. Since the robot's detection efficiency and endurance are primarily evaluated based on the total path length and energy consumption, detection efficiency was determined by the total path length; the shorter the path, the higher the efficiency of the robot in completing the coverage task. A lower repetition rate indicated that the robot avoided redundant cleaning or detection during the task, thereby improving coverage efficiency.

For the robot used in the experiment, the energy consumption of a 45° rotation is approximately twice that of moving one unit length. The number of turns and the corresponding turning angles both directly affect the energy consumption during the detection process. Therefore, we primarily consider the total path length, the number of turns, the repetition rate, and the energy consumption. Each unit of path length corresponds to an actual movement distance of 100 mm, and each unit of energy consumption is approximately 1.2 J. The data obtained are shown in Table 1.

Table 1. Performance Comparison Between the Traditional BINN Algorithm and the Improved BINN Algorithm.

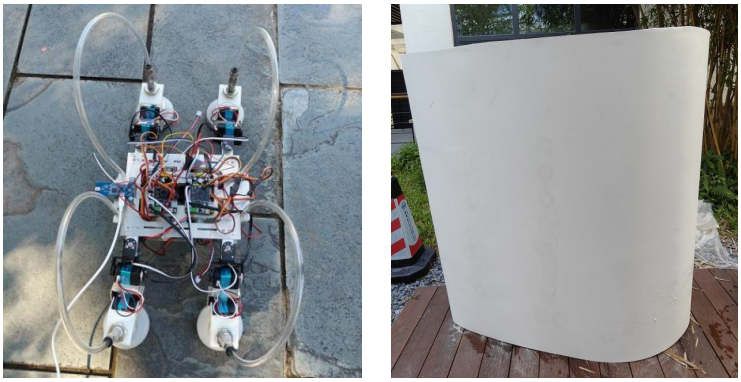
Algorithm Type	Total Path Length (mm)	Number of Turns	Repetition Rate	Energy Consumption (J)
Traditional BINN algorithm	39,748	113	0.035	1015.2
Improved BINN algorithm	39,270	121	0.023	979.2

By comparison, it can be observed that under the consideration of energy consumption, the improved BINN full coverage path planning algorithm achieves a shorter total path length and lower repetition rate compared to the traditional BINN full coverage path planning algorithm. Since energy consumption information is taken into account, the robot tends to move toward areas with lower energy costs. As a result, the number of turns increases; however, because a 90° turn requires multiple incremental rotations, the actual energy consumption is reduced.

This indicates that, when energy consumption is considered, the improved BINN full coverage path planning algorithm achieves better results in terms of the robot's endurance and operational efficiency.

4. Prototype Experiment

The wall-climbing robot used in this study is based on a prototype of a quadruped wall-climbing robot. The robot achieves adhesion and movement on wind turbine blades through the use of an air pump. Various sensor modules are mounted on the robot. The physical robot is shown in Figure 14a.



(**a**) (**b**)

Figure 14. Experimental Platform for Algorithms. (**a**) Wall-climbing robot prototype. (**b**) Experimental platform for typical wind turbine blade regions.

Due to the large overall size of wind turbine blades, which can reach lengths of hundreds of meters, it is challenging to conduct full-scale machining and experiments on the entire blade. However, proportionally downsizing the blade often leads to an increase in curvature, which does not meet the actual operational requirements. Therefore, a 1:1 scale model of a wind turbine blade's typical working region was selected as the experimental platform. This approach not only simulates the real working environment but also represents the most challenging area for the wall-climbing robot to operate.

The selected wind turbine blade experimental platform is shown in Figure 14b. The platform is made of fiberglass, the same material as actual wind turbine blades, which further enhances the simulation of real working conditions. The experimental platform measures approximately 1.5 m × 1.5 m and features curved surfaces with varying curvatures, making it suitable for various performance tests.

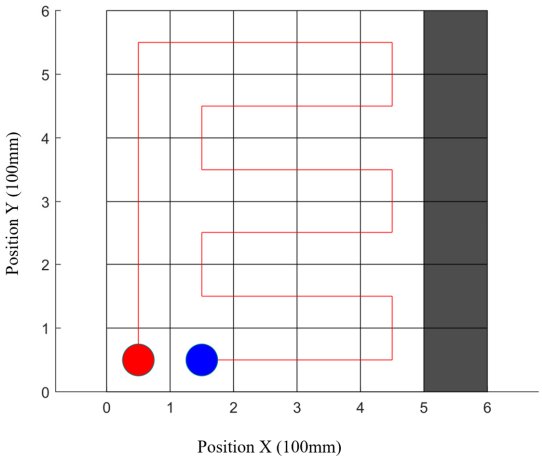
In the experiment for the full coverage path planning algorithm, considering the size of the wall-climbing robot and the actual range of the wind turbine blade, an area of 1.2 m × 1.2 m on the experimental platform was selected for path planning testing. Each grid cell was set to a size of 200 mm × 200 mm. The resulting 2.5D grid map of the experimental platform is shown in Figure 15.

Assuming the far-right area is an inaccessible region, simulation tests were conducted using both the BINN algorithm and the improved BINN algorithm. The robot starts from

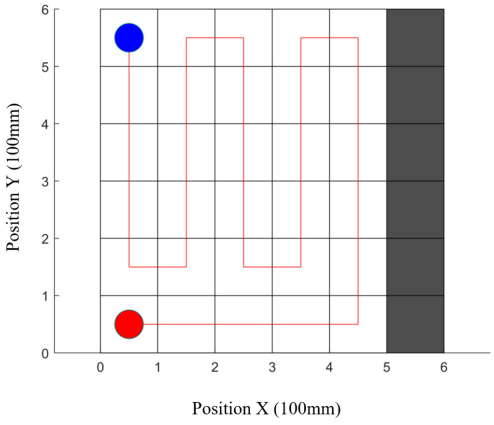
the bottom-left grid and performs full coverage path planning. The resulting simulated paths are shown in Figure 16a,b.

110	193	257	303	317	256
121	202	265	309	323	264
132	210	272	317	330	270
141	218	280	324	337	276
150	226	286	331	343	282
157	232	293	336	348	287

Figure 15. 2.5D Grid Map of the Experimental Platform.



(**a**)



(**b**)

Figure 16. Comparison of Movement Paths Between Two BINN Algorithms. (The red circle indicates the starting point, and the blue circle indicates the endpoint.) (**a**) Simulation Results of Full Coverage Path Planning Using the Basic BINN Algorithm. (**b**) Simulation Results of Full Coverage Path Planning Using the Improved BINN Algorithm.

The simulation data obtained from the tests are shown in Table 2. The improved BINN full coverage path planning algorithm demonstrates significant advantages in obstacle-free environments, particularly in reducing the number of turns and energy consumption. Since

most of the wind turbine blade consists of obstacle-free feasible areas with only a small portion being inaccessible, this optimization improves the robot's operational efficiency and endurance. Additionally, the obstacle avoidance capability and advantages of the improved BINN algorithm for inaccessible areas have been validated in Section 4. This indicates that the improved BINN algorithm can also achieve excellent path planning results in complex environments.

Table 2. Comparison of Algorithm Simulation Results for Experimental Wind Turbine Blade.

Algorithm Type	Total Path Length (mm)	Number of Turns	Repetition Rate	Energy Consumption (J)
Traditional BINN algorithm	580	11	0	175.2
Improved BINN algorithm	580	9	0	156

Conducting practical tests of the wall-climbing robot on the wind turbine blade experimental platform is a crucial step in validating the effectiveness of its path planning algorithm and motion stability. The experimental process is shown in Figure 17, which fully demonstrates part of the process where the robot moves along the planned path on the surface of the wind turbine blade. During the test, the robot primarily performs the following three types of action: lateral movement, vertical movement, and self-rotation. The entire experimental testing process showcases the robot's ability to execute the path planning algorithm and adapt to real-world environments, verifying its coverage performance on complex curved surfaces.

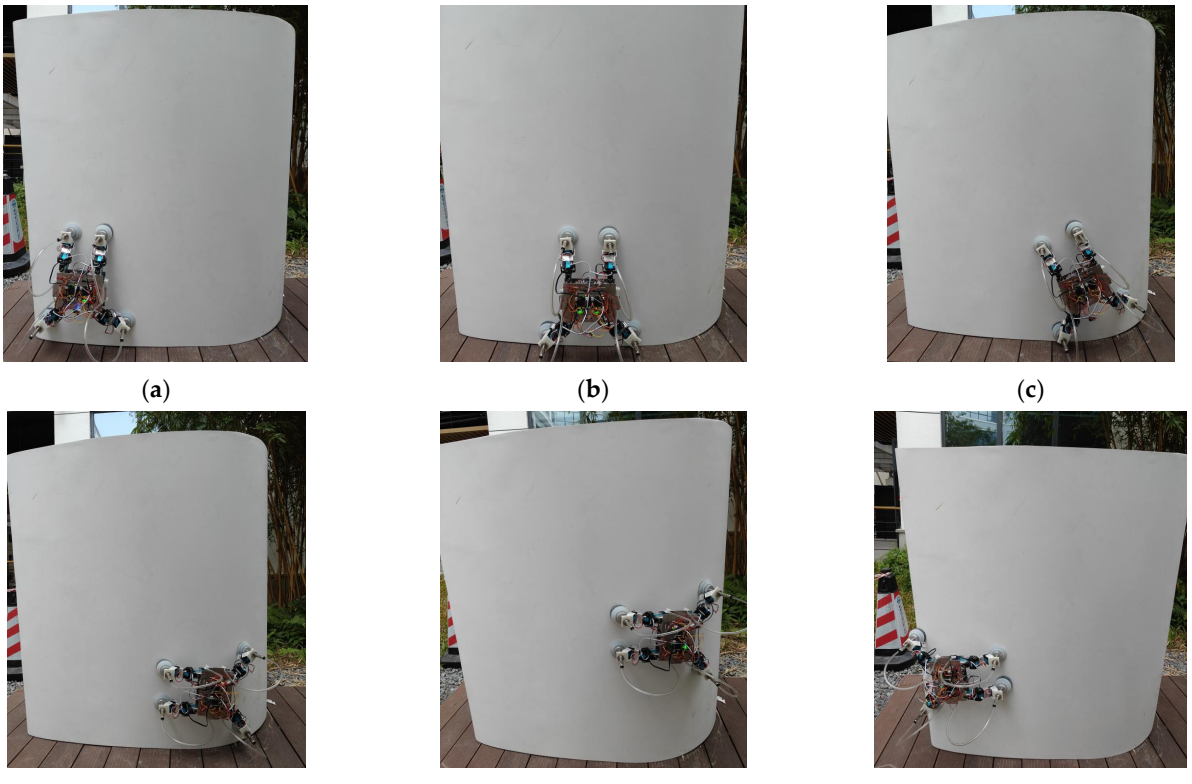


Figure 17. Wall-climbing robot moves along the planned path. (**a**) Starting point; (**b**) Lateral movement; (**c**) Self-rotation; (**d**) Rotation completed; (**e**) Upward movement; (**f**) Downward movement.

5. Conclusions

Through the integration of advanced path planning algorithms with motion control strategies, the wall-climbing robot demonstrates strong adaptability and stability on complex surfaces. The established path planning system ensures efficient coverage of the wind turbine blade while maintaining low energy consumption and avoiding unnecessary movements. The proposed algorithms, especially the improved BINN algorithm, can be easily applied to similar robotic applications with minimal adjustments, showcasing the method's versatility. The testing process validates the feasibility of the system in real-world scenarios, achieving end-to-end path execution without relying heavily on manual intervention or preprocessing.

In addition, the following shortcomings and future prospects have been identified:

The method relies on a prior model of the environment, making it effective for known 3D environments like wind turbine blades. However, for targets without prior models, environment perception and point cloud data collection are necessary. In complex curved surfaces, the further optimization of motion efficiency and stability is needed, especially in scenarios with closely clustered obstacles. Additionally, enhancing the robot's adaptability to unexpected environmental changes, integrating real-time feedback and predictive modeling, and employing higher-precision motors alongside advanced closed-loop control algorithms for motion and inspection tasks could significantly improve coverage accuracy, operational efficiency, and overall system reliability.

Author Contributions: Conceptualization, D.C., G.Y. and S.H.; methodology, D.C.; software, D.C.; validation, D.C., G.Y. and S.H.; investigation, D.C.; resources, G.Y.; data curation, D.C. and S.H.; writing—original draft preparation, D.C.; writing—review and editing, D.C., G.Y. and S.H.; visualization, D.C. and S.H.; supervision, G.Y.; project administration, G.Y. All authors have read and agreed to the published version of the manuscript.

Funding: This research received no external funding.

Data Availability Statement: Data are contained within the article.

Acknowledgments: The authors wish to express their sincere gratitude to everyone who has provided assistance and support.

Conflicts of Interest: The authors declare no conflicts of interest.

References

1. Kara, T.; Şahin, A.D. Implications of Climate Change on Wind Energy Potential. *Sustainability* **2023**, *15*, 14822. [CrossRef]
2. Su, X.; Wang, X.; Xu, W.; Zhang, Y. Offshore Wind Power: Progress of the Edge Tool, Which Can Promote Sustainable Energy Development. *Sustainability* **2024**, *16*, 7810. [CrossRef]
3. Wu, J.; Xiao, J.; Hou, J.; Zhang, L. Development Potential Assessment for Wind and Photovoltaic Power Energy Resources in the Main Desert–Gobi–Wilderness Areas of China. *Energies* **2023**, *16*, 4559. [CrossRef]
4. Hansen, T.A.; Wilson, E.J.; Fitts, J.P.; Johnson, M. Five Grand Challenges of Offshore Wind Financing in the United States. *Energy Res. Soc. Sci.* **2024**, *107*, 103329. [CrossRef]
5. Kong, K.; Dyer, K.; Payne, C.; Zhang, X. Progress and Trends in Damage Detection Methods, Maintenance, and Data-Driven Monitoring of Wind Turbine Blades–A Review. *Renew. Energy Focus* **2023**, *44*, 390–412. [CrossRef]
6. Agrawal, S.; Corley, I.; Wallace, C.; Smith, J. Barely-Visible Surface Crack Detection for Wind Turbine Sustainability. In Proceedings of the 2024 IEEE/RSJ International Conference on Intelligent Robots and Systems (IROS), Abu Dhabi, The United Arab Emirates, 14–18 October 2024; IEEE: New York, NY, USA, 2024; pp. 5933–5939. [CrossRef]
7. Car, M.; Markovic, L.; Ivanovic, A.; Vasiljevic, N. Autonomous Wind-Turbine Blade Inspection Using Lidar-Equipped Unmanned Aerial Vehicle. *IEEE Access* **2020**, *8*, 131380–131387. [CrossRef]
8. Sattar, T.P.; Leon Rodriguez, H.; Bridge, B. Climbing Ring Robot for Inspection of Offshore Wind Turbines. *Ind. Robot Int. J.* **2009**, *36*, 326–330. [CrossRef]

9. Elkmann, N.; Felsch, T.; Förster, T. Robot for Rotor Blade Inspection. In Proceedings of the 2010 1st International Conference on Applied Robotics for the Power Industry, Montreal, QC, Canada, 5–7 October 2010; IEEE: New York, NY, USA, 2010; pp. 1–5. [CrossRef]
10. Lee, D.G.; Oh, S.; Son, H.I. Maintenance Robot for 5-MW Offshore Wind Turbines and Its Control. *IEEE/ASME Trans. Mechatron.* **2016**, *21*, 2272–2283. [CrossRef]
11. Jiang, Z.; Jovan, F.; Moradi, P.; Wan, Z.; Zhang, Y. A Multirobot System for Autonomous Deployment and Recovery of a Blade Crawler for Operations and Maintenance of Offshore Wind Turbine Blades. *J. Field Robot.* **2023**, *40*, 73–93. [CrossRef]
12. Cieslak, C.; Shah, A.; Clark, B.; Smith, J.; Taylor, R. Wind-Turbine Inspection, Maintenance, and Repair Robotic System. In *Turbo Expo: Power for Land, Sea, and Air, Proceedings of the ASME Turbo Expo 2023: Turbomachinery Technical Conference and Exposition, Boston, MA, USA, 26–30 June 2023*; American Society of Mechanical Engineers (ASME): New York, NY, USA, 2023; Volume 14, p. V014T37A004. [CrossRef]
13. Zhang, K.; Pakrashi, V.; Murphy, J.; O'Sullivan, J. Inspection of Floating Offshore Wind Turbines Using Multi-Rotor Unmanned Aerial Vehicles: Literature Review and Trends. *Sensors* **2024**, *24*, 911. [CrossRef]
14. Yakoubi, M.A.; Laskri, M.T. The Path Planning of Cleaner Robot for Coverage Region Using Genetic Algorithms. *J. Innov. Digit. Ecosyst.* **2016**, *3*, 37–43. [CrossRef]
15. Lakshmanan, A.K.; Mohan, R.E.; Ramalingam, B.; Thangavel, P. Complete Coverage Path Planning Using Reinforcement Learning for Tetromino-Based Cleaning and Maintenance Robot. *Autom. Constr.* **2020**, *112*, 103078. [CrossRef]
16. Pour Arab, D.; Spisser, M.; Essert, C. Complete Coverage Path Planning for Wheeled Agricultural Robots. *J. Field Robot.* **2023**, *40*, 1460–1503. [CrossRef]
17. Wu, X.; Bai, J.; Hao, F.; Zhang, L.; Li, Y. Field Complete Coverage Path Planning Based on Improved Genetic Algorithm for Transplanting Robot. *Machines* **2023**, *11*, 659. [CrossRef]
18. Ma, C.; Zou, H.; An, X. A Complete Coverage Path Planning Approach for an Autonomous Underwater Helicopter in Unknown Environment Based on VFH+ Algorithm. *J. Mar. Sci. Eng.* **2024**, *12*, 412. [CrossRef]
19. Bao, H.; Wang, Y.; Zhu, H.; Zhang, J.; Li, X. Area Complete Coverage Path Planning for Offshore Seabed Organisms Fishing Autonomous Underwater Vehicle Based on Improved Whale Optimization Algorithm. *IEEE Sens. J.* **2024**, *14*, 495. [CrossRef]
20. Barraquand, J.; Latombe, J.C. Robot Motion Planning: A Distributed Representation Approach. *Int. J. Robot. Res.* **1991**, *10*, 628–649. [CrossRef]
21. Choset, H. Coverage of Known Spaces: The Boustrophedon Cellular Decomposition. *Auton. Robot.* **2000**, *9*, 247–253. [CrossRef]
22. Acar, E.U.; Choset, H.; Rizzi, A.A.; Atkar, P.N.; Hull, D. Morse Decompositions for Coverage Tasks. *Int. J. Robot. Res.* **2002**, *21*, 331–344. [CrossRef]
23. Huang, W.H. Optimal Line-Sweep-Based Decompositions for Coverage Algorithms. In Proceedings of the 2001 ICRA: IEEE International Conference on Robotics and Automation (Cat. No. 01CH37164), Seoul, Republic of Korea, 21–26 May 2001; IEEE: New York, NY, USA, 2001; Volume 1, pp. 27–32. [CrossRef]
24. De Carvalho, R.N.; Vidal, H.A.; Vieira, P.; Gomide, F. Complete Coverage Path Planning and Guidance for Cleaning Robots. In Proceedings of the ISIE'97: IEEE International Symposium on Industrial Electronics, Guimarães, Portugal, 7–11 July 1997; IEEE: New York, NY, USA, 1997; Volume 2, pp. 677–682. [CrossRef]
25. Moravec, H.; Elfes, A. High-Resolution Maps from Wide Angle Sonar. In Proceedings of the 1985 IEEE International Conference on Robotics and Automation, St. Louis, MO, USA, 25–28 March 1985; IEEE: New York, NY, USA, 1985; Volume 2, pp. 116–121. [CrossRef]
26. Miao, C.; Chen, G.; Yan, C.; Wu, Y. Path planning optimization of indoor mobile robot based on adaptive ant colony algorithm. *Comput. Ind. Eng.* **2021**, *156*, 107230. [CrossRef]
27. Nazarahari, M.; Khanmirza, E.; Doostie, S. Multi-objective multi-robot path planning in continuous environment using an enhanced genetic algorithm. *Expert Syst. Appl.* **2019**, *115*, 106–120. [CrossRef]
28. Ariyanto, M.; Refat, C.M.M.; Hirao, K.; Morishima, K. Movement optimization for a cyborg cockroach in a bounded space incorporating machine learning. *Cyborg Bionic Syst.* **2023**, *4*, 0012. [CrossRef] [PubMed]
29. Takanashi, T.; Nakajima, M.; Takemori, T.; Tanaka, M. Obstacle-aided locomotion of a snake robot using piecewise helixes. *IEEE Robot. Autom. Lett.* **2022**, *7*, 10542–10549. [CrossRef]
30. Brambilla, M.; Ferrante, E.; Birattari, M.; Dorigo, M. Swarm robotics: A review from the swarm engineering perspective. *Swarm Intell.* **2013**, *7*, 1–41. [CrossRef]
31. Tan, X.; Han, L.; Gong, H.; Wang, Y.; Li, J. Biologically Inspired Complete Coverage Path Planning Algorithm Based on Q-Learning. *Sensors* **2023**, *23*, 4647. [CrossRef]
32. Zhu, D.; Zhou, B.; Yang, S.X. A Novel Algorithm of Multi-AUVs Task Assignment and Path Planning Based on Biologically Inspired Neural Network Map. *IEEE Trans. Intell. Veh.* **2020**, *6*, 333–342. [CrossRef]
33. Luo, C.; Yang, S.X.; Li, X.; Li, J. Neural-Dynamics-Driven Complete Area Coverage Navigation through Cooperation of Multiple Mobile Robots. *IEEE Trans. Ind. Electron.* **2016**, *64*, 750–760. [CrossRef]

34. Grossberg, S. Nonlinear neural networks: Principles, mechanisms, and architectures. *Neural Netw.* **1988**, *1*, 17–61. [CrossRef]
35. Xu, W.L.; Pap, J.S.; Bronlund, J. Design of a biologically inspired parallel robot for foods chewing. *IEEE Trans. Ind. Electron.* **2008**, *55*, 832–841. [CrossRef]
36. Muthugala, M.A.V.J.; Samarakoon, S.M.B.P.; Elara, M.R. Toward Energy-Efficient Online Complete Coverage Path Planning of a Ship Hull Maintenance Robot Based on Glasius Bio-Inspired Neural Network. *Expert Syst. Appl.* **2022**, *187*, 115940. [CrossRef]
37. Yang, S.X.; Luo, C. A neural network approach to complete coverage path planning. *IEEE Trans. Syst. Man Cybern. Part B (Cybern.)* **2004**, *34*, 718–724. [CrossRef]

Disclaimer/Publisher's Note: The statements, opinions and data contained in all publications are solely those of the individual author(s) and contributor(s) and not of MDPI and/or the editor(s). MDPI and/or the editor(s) disclaim responsibility for any injury to people or property resulting from any ideas, methods, instructions or products referred to in the content.